communications physics

ARTICLE

https://doi.org/10.1038/s42005-022-00938-8 OPEN

# Gain-switching in $CsPbBr_3$ microwire lasers

Jiao Tian[1,3], Guoen Weng[1,3✉], Yuejun Liu[1,3], Shengjie Chen[1], Fuyi Cao[1], Chunhu Zhao[1], Xiaobo Hu[1], Xianjia Luo[1], Junhao Chu[1], Hidefumi Akiyama[2] & Shaoqiang Chen[1,2✉]

All-inorganic perovskite microwire lasers, which have intrinsic high material gain and short cavity, especially favor the generation of ultrashort optical pulses via gain switching for various potential applications. Particularly, the ultrashort gain-switched pulses may extend perovskite microwires to previously inaccessible areas, such as ultrafast switches, and chipscale microcombs pumping souces in photonic integrated circuits. Here, we show 13.6-ps ultrashort single-mode green pulses from the gain-switched $CsPbBr_3$ microwire lasers under femtosecond optical pumping. The gain-switching dynamics is experimentally investigated by a streak camera system. The excitation fluence dependences of pulse width, delay time and rise time of the output pulses show good agreements with the rate equation simulations with taking gain nonlinearities and carrier recombination *ABC* model into account. Our results reveal that perovskite microwire lasers have potential for ultrashort pulse generation, while the low transient saturated gain, which may result from the high transient carrier temperature under femtosecond pumping is a significant limitation for further pulse shortening.

[1] State Key Laboratory of Precision Spectroscopy, Department of Electronic Engineering, East China Normal University, 500 Dongchuan Road, Shanghai 200241, China. [2] Institute for Solid State Physics, The University of Tokyo, 5-1-5 Kashiwanoha, Kashiwa, Chiba 277-8581, Japan. [3] These authors contributed equally: Jiao Tian, Guoen Weng, Yuejun Liu. ✉email: egweng@ee.ecnu.edu.cn; sqchen@ee.ecnu.edu.cn

Over the past few years, micro/nanostructured all-inorganic semiconductor perovskites hold great promises as microscale light source for potential application in photonic integrated systems due to their extraordinary optoelectronic properties[1–5]. Substantial research on lasing emission from cesium lead halide perovskites with diverse morphologies, including nanowires[6], nanosheets[7], microspheres[8], microdisks[9] and quantum dots[10], has been conducted under optical pumping. Related photophysics involved in the stimulated emission has also been explored in Fabry–Pérot cavity[11–14] and whispering-gallery-mode cavity[15–18]. Among the $CsPbX_3$ (X=Cl, Br, and I) perovskites, the superior stability and better quantum efficiency render the bromide counterparts very promising in the next generation green-emitting devices. Particularly, the short green laser pulses with high peak energies are always highly required for medical treatment and underwater communication[19,20]. To date, despite a plethora of publications on lasing action in $CsPbBr_3$ perovskites, it remains rare to establish concern on how to achieve the short pulse from such material system.

At present, three major techniques have been employed to generate short laser pulses from semiconductor lasers, including mode-locking, *Q*-switching and gain-switching techniques. Gain-switching technique is a very simple method for short-pulse generation via directly modulating optical gain in semiconductor lasers. It requires neither complicated laser systems, delicate alignment, nor elaborate device structures[21,22], and the output pulse frequency can be modulated freely by an external pump source with tunable frequency. The gain-switched pulse width can be compressed to a few picoseconds (ps) by applying post-processing techniques, such as pulse shaping[23], spectral filtering[24], and pulse compression[25,26]. Gain-switched pulses with duration from several to hundreds of ps have been obtained in various semiconductor lasers using above techniques or even without any post-processing[27–31], and even sub-picosecond pulses have been obtained recently via gain-switching and spectral-filtering techniques[32]. Compared to the conventional II–VI and III–V semiconductor compounds systems, lead halide perovskite microcavity lasers exhibit higher optical gain and shorter photon lifetime, making it more fascinating for the ultrashort pulses generation through gain-switching. However, investigation on gain-switching characteristics in a perovskite laser is still lacking in spite of its great value in practical applications. Generally, a kinetic rate equations model is utilized to study the fundamental electrical and photophysical kinetics in gain-switched process, where the optical gain is usually assumed to be linearly related to the carrier density[33]. The recent studies, however, have revealed strong gain-saturation nonlinearity, especially under strong pumping conditions[33,34]. Moreover, it has been demonstrated that carrier recombination processes play an important role during gain-switching[35]. The carrier recombination rate $R$ can be characterized by a function of carrier densities $n$ with $ABC$ coefficients, the so called $ABC$ model, i.e., $R(n) = An + Bn^2 + Cn^3$, where $A$, $B$, and $C$ are Shockley–Read–Hall ($SRH$), radiative, and Auger coefficients, respectively. Consequently, the gain-saturation nonlinearity and the $ABC$ model should be introduced into the rate equation model to comprehensively understand the carrier kinetics and short pulse generation mechanism during gain-switching processes.

In this work, we reported single-mode laser operations in $CsPbBr_3$ microwires under femtosecond (fs) optical pumping. The short pulses of dozen ps were experimentally obtained by excitation-fluence dependent time-resolved photoluminescence (TRPL). Clear gain-switching mechanism for the short pulses generation were revealed. With taking the gain nonlinearities and the carrier recombination $ABC$ model into account, the gain-switching characteristics and dynamics of short pulses from the $CsPbBr_3$ microwires were semi-quantitively simulated at elevated pump levels based on a modified rate equation model. It was found that the low transient saturated gain of $CsPbBr_3$ microwires under gain-switching operations greatly affected the generation of shorter optical pulse, and the carrier heating could be a possible reason accounting for the low saturated gain. Our study opens the door of gain switching for perovskite lasers and provides a significant guidance for understanding generation dynamics and limit factors of short pulses, which are very important for real-world applications, such as optical storage[36], ultrafast optical communication[30], bioimaging[31], and time-resolved spectroscopy[37].

## Results and discussion

**Synthesis and characterization of $CsPbBr_3$ microwires**. The $CsPbBr_3$ perovskite microwires were synthetized by a liquid-phase self-assembled growth method on a sapphire ($Al_2O_3$) substrate. The top-view scanning electron microscopy (SEM) images in Fig. 1a, b show that the microstructures of as-grown

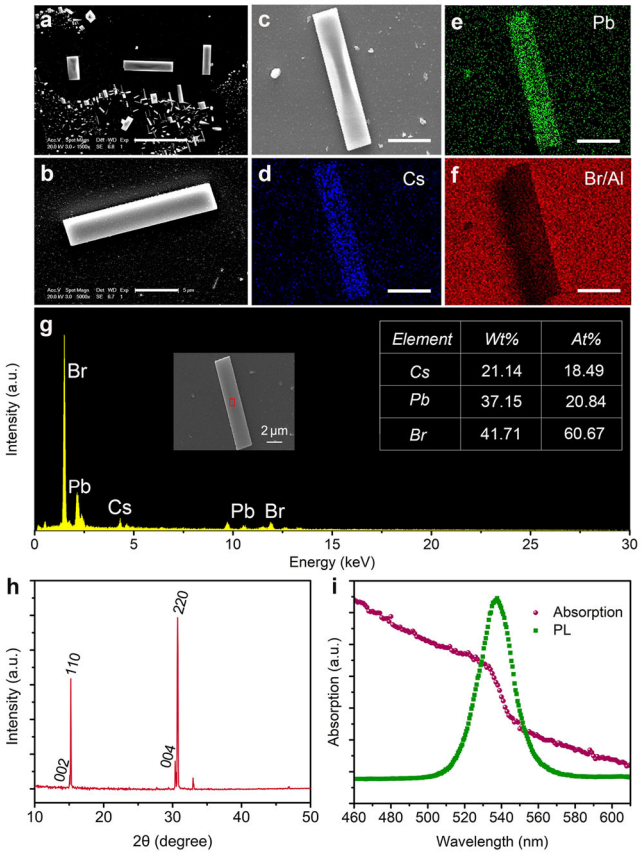


**Fig. 1 Characterizations of the synthesized $CsPbBr_3$ perovskite microwires. a**, **b** Scanning electron microscopy images of $CsPbBr_3$ microwires. Scale bars in **a** and **b** are 20 and 5 μm, respectively. Element mapping of Cs (**d**), Pb (**e**) and Br (**f**) for the corresponding individual $CsPbBr_3$ microwire in **c**. Scale bars in **c**–**f** are 5 μm. Here, the background of the element mapping signals is black in color, while the element signals of Cs, Pb, and Br are blue, green, and red, respectively. Because of the similar detection energies for Br and Al, which comes from the $Al_2O_3$ substrate, the signal intensity of Br for $CsPbBr_3$ microwire seems to be lower than that for substrate area. While the energy dispersive X-ray spectroscopy analysis shows that the atomic ratios of Cs, Pb and Br within the investigated microwires are in good agreement with the ideal 1:1:3 stoichiometry of $CsPbBr_3$. **g** Energy dispersive X-ray spectroscopy analysis of the $CsPbBr_3$ microwire. The red rectangular region of the inset shows the measured area. **h** X-ray diffraction pattern of the $CsPbBr_3$ microwires. **i** Absorption and photoluminescence (PL) spectra of the $CsPbBr_3$ microwires.

$CsPbBr_3$ perovskite are dominated by microwires with smooth, clean surface and edge, indicating the excellent crystalline quality of the $CsPbBr_3$ microwires. The lengths of the wires range from ten to several tens of microns, and the widths are a few microns. From the elemental mapping shown in Fig. 1c–f, it can be observed that the three elements of Cs, Pb, Br are evenly distributed in the individual $CsPbBr_3$ perovskite microwire. And the energy dispersive X-ray spectroscopy (EDS) analysis presented in Fig. 1g reveals that the atomic ratios of Cs, Pb and Br are 18.49:20.84:60.67, which performs a good agreement with the ideal 1:1:3 stoichiometry of $CsPbBr_3$. The X-ray diffraction (XRD) measurement has also been carried out for the $CsPbBr_3$ microwires, as shown in Fig. 1h. It is found that the $CsPbBr_3$ possesses the orthorhombic crystal phase which can be identified by the clear diffraction peak splitting. Figure 1i shows typical absorption and room-temperature photoluminescence (PL) spectra of the $CsPbBr_3$ microwires. A clear absorption edge around 530 nm and a strong PL emission centered at 536 nm are revealed, which are consistent with previous studies[38].

**Single-mode laser emissions from $CsPbBr_3$ microwires**. To explore the potential of $CsPbBr_3$ microwires for laser application, an individual $CsPbBr_3$ microwire was optically pumped by 400-nm fs pulse at room temperature. Figure 2a presents the dark-field optical image of the individual microwire at a low excitation intensity below the lasing threshold. The corresponding images at threshold and above threshold are respectively shown in Fig. 2b, c. It can be seen that the emission intensity below threshold was almost uniform for the whole individual microwire while above threshold the coherent green light was emitted from the two end-facets, indicating the transition from spontaneous emission to Fabry–Pérot mode stimulated radiation. Figure 2d displays the emission spectra evolution for the investigated $CsPbBr_3$ microwire at various excitation intensities. The spectra are vertically offset for clarity. Under low excitation intensity, only a predominant broad luminescence, characteristic of spontaneously emitted light centered at near 536 nm can be observed. As excitation energy increased to 37.2 μJ $cm^{-2}$, a distinctive narrow peak at about 544 nm emerges at the low energy side of the spectrum, and grows rapidly with the continued increase of pumping fluence. Moreover, the single narrow peak still persisted even at elevated excitation intensity. Usually, most of microscale wires are subject to random fluctuations and instabilities, showing typical multimode lasing. Here, an unambiguous single-mode lasing was achieved owing to the high-quality laser cavity formed by the smooth crystal end-facets. The plots of integrated emission intensity and the full width at half maximum (FWHM) versus excitation density are shown in Fig. 2e. The log-log "S-shaped" curve and linewidth narrowing clearly confirm the lasing action very well. The lasing threshold ($P_{th}$) is accordingly derived to be 37.2 μJ $cm^{-2}$, and the FWHM below and above the threshold are around 30 and 0.21 nm, respectively. Meanwhile, the spontaneous emission coupling factor $\beta$ can be extracted from the "S" curve to be about 0.09. The enlarged spectra in Fig. 2f disclose that blueshift and spectral broadening occur as the pump intensity increases. Generally, there are many origins may result in the peak shift, such as electron/hole many-body interactions, band filling, thermally induced refractive index change and optical density fluctuations[39,40], which will be discussed in more details in the latter section. Based on the relationship of $Q = \lambda/\delta\lambda$, where $Q$, $\lambda$ and $\delta\lambda$ are cavity quality factor, peak wavelength and FWHM, respectively, we calculated the $Q$ factors at

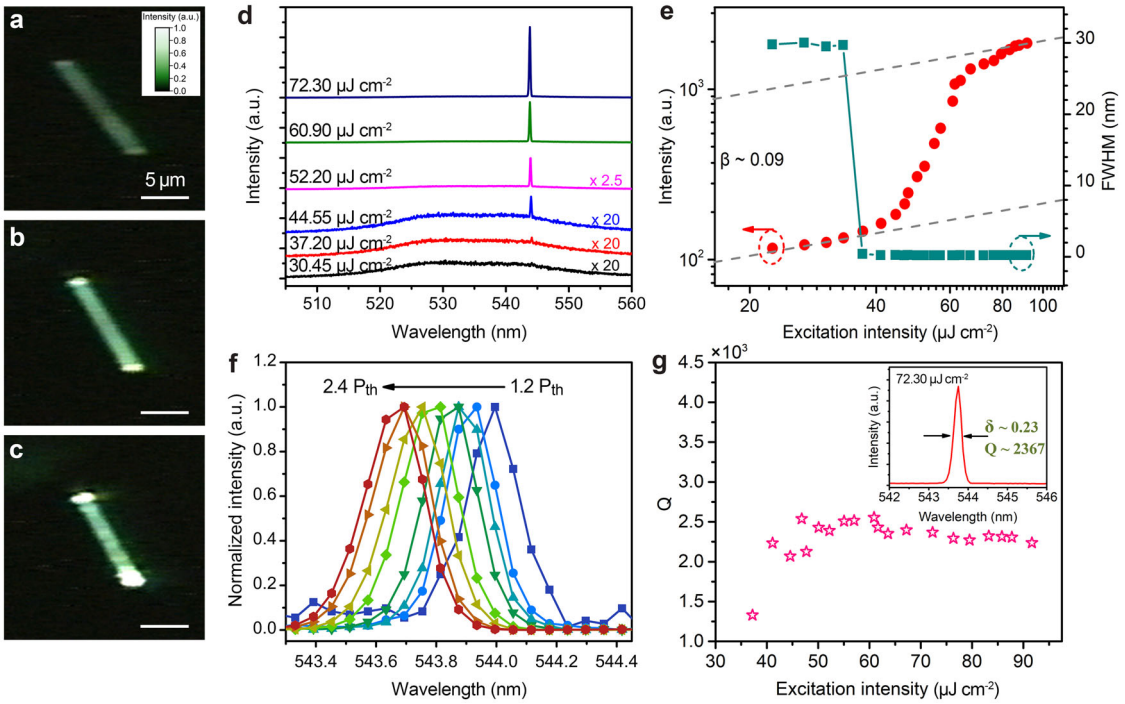


**Fig. 2 Lasing characteristics of individual $CsPbBr_3$ microwire.** Optical images of luminescence signal below threshold (**a**), at threshold (**b**) and above threshold (**c**) under 400-nm fs excitation. Scale bars in **a**–**c** are 5 μm. **d** Emission spectra of $CsPbBr_3$ microwires at different pump fluences. For clarity, the curves have been vertically shifted and some of them are magnified. **e** Integrated emission intensity (red circles) and full width at half maximum (FWHM, cyan squares) versus excitation energy density. The error bars that represent the standard deviation from the mean are too small to be visible. The representative kink behavior is exhibited and the lasing threshold is derived to be about 37.2 μJ $cm^{-2}$. The spontaneous emission coupling factor $\beta$ is estimated to be ~0.09 from the "S-shaped" curve. **f** Enlarged spectra with various excitation energy from 1.2 to 2.4 $P_{th}$. **g** The $Q$ factors at various excitation fluences above the lasing threshold. The error bars here are too small to be visible. Inset is the lasing spectrum at a pump fluence of 72.3 μJ $cm^{-2}$ with a emission peak at 543.8 nm and a FWHM ($\delta\lambda$) of about 0.23 nm, corresponding to a $Q$ factor of ~2367.

various excitation fluences. As shown in Fig. 2g, with increasing the excitation level, the $Q$ factor gradually increases and finally saturates to a maximum value of ~2500. For example, the inset of Fig. 2g illustrates the FWHM of ~0.23 nm for the lasing mode at 543.8 nm at a pump fluence of 72.3 μJ cm$^{-2}$, corresponding to a relatively high $Q$ factor of ~2367. The maximum value of $Q$ factor is higher than those recently reported in some $CsPbBr_3$ microstructures[41,42], which can be ascribed to the excellent crystal quality of the as-synthesized $CsPbBr_3$ perovskites. Here, the spontaneous emission coupling factor $\beta$ is relavant to the photon radiation process as decribed in our rate equation model. The $Q$ factor can also be described by $Q = \frac{2\pi}{\lambda}\frac{n_g}{g_{th}}$[43], where $n_g$ is the group index of refraction and $g_{th}$ is the threshold gain. Theoretical simulations show that with decreasing differential gain $g_0$ and/or saturated gain $g_s$ or increasing the transparent carrier density $n_0$ while fixing other material parameters, the lasing threshold value increases monotonously, resulting in the change in $Q$-value according to the expression. That is to say, the lasing threshold and the $Q$ factor are physically determined by the material parameters as well as the cavity structure under gain-switching operations.

**Gain-switching dynamics in $CsPbBr_3$ microwires**. The gain of a semiconductor laser can be switched from a state below threshold into inversion by directly modulating the pump pulse intensity, and then the laser produces stimulated emission. Generally, a larger lasing threshold means more difficult to establish the population inversion and the consequent stimulated emission with ultrashor pulse width. Thus, if the threshold value increases, the difficulty in establishing gain-switching is then dramatically increased, and an additional bias voltage is necessary to help to establish the population inversion quickly. On the other hand, a higher threshold means a higher operating temperature, which could deteriorate the pulse stability under gain-switching. To gain insight into the gain-switched lasing characteristics and dynamics of $CsPbBr_3$ microwires, the excitation-intensity-dependent TRPL were performed using a streak-camera system. Figure 3a–d shows the single-mode TRPL images and the corresponding linear plots of the spectrally integrated pulse waveforms of the $CsPbBr_3$ microwires at various excitation intensities above the lasing threshold (additional images are provided in Supplementary Note 1, Supplementary Figs. 1 and 2). All the output pulse started after the excitation pulse has ended, indicating the efficient gain switching. It can be obviously seen that time interval between the excitation and emission pulses, called delay time, gradually decreases as the excitation intensity increases. This phenomenon is one of the emblematic gain-switching properties, which have been widely demonstrated experimentally and theoretically in various gain-switched semiconductor lasers[27,36,44–46]. Here, it is worth noting that the measured 4.95-ps pulse width of the fs pump pulse shown in Fig. 3e is due to setup-resolution limit of the streak camera. In our scenarios, the pulse widths of the output emissions are all shorter than 19 ps with delay times smaller than 40 ps. The generation of short pulse without any post-processing indicates the superior potentiality of $CsPbBr_3$ microstructures as ultrafast light sources. Besides, the spectral broadening and peak blue-shift with increasing pump density are unambiguously observed, which coincides with the time-integrated spectroscopy shown in Fig. 2. The blue-shift at higher excitation fluence can be interpreted by the transient reduction of refractive index with the increase of carrier density in the ultrafast pump case. It can also be seen from the streak camera that the wavelength of the emission pulses presents almost linearly dependence on time decay, that is, the entire gain-switched pulses were linearly down-chirped.

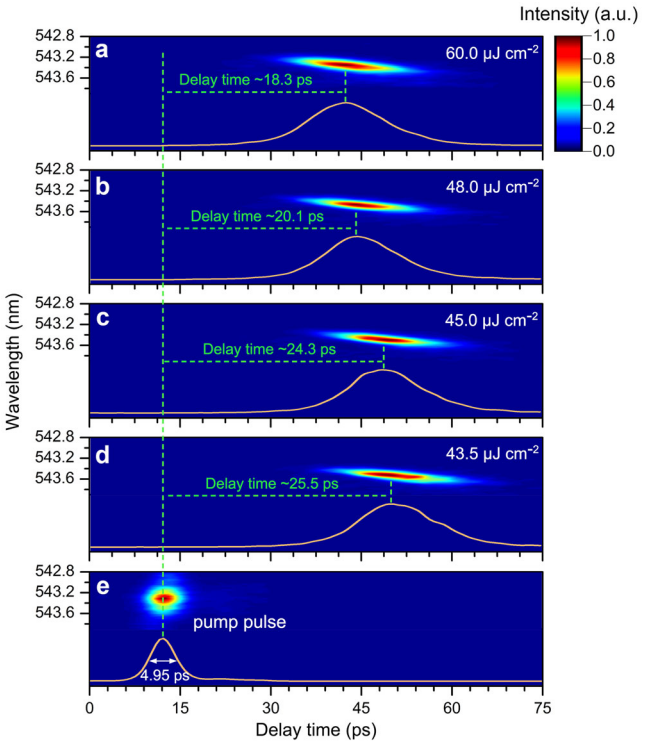


**Fig. 3 Excitation-intensity-dependent time-resolved photoluminescence.** **a–d** Temporally- and spectrally-resolved streak-camera images, and the corresponding spectral-integrated waveforms of output gain-switched lasing pulses from $CsPbBr_3$ microwires for various excitation fluences above the lasing threshold. The excitation fluences are respectively displayed in the top-right of the graphs, varying from 43.5 to 60.0 μJ cm$^{-2}$. **e** Streak-camera image of the fs pump pulses. The measured 4.95-ps pulse width of the fs pulse is due to the limit of setup-resolution. The plotted time window of each single streak-camera image is 75 ps.

The chirp renders the spectral and pulse width broadening, hindering the generation of shorter pulse. Figure 4a performs the spectral property of the gain-switched pulse at 60 μJ cm$^{-2}$ and the corresponding streak-camera image in the inset. The delay time increases almost linearly with the increase of wavelength (linear down chirp) with a slope of 41.5 ps nm$^{-1}$. In gain switching process, the chirp is inevitable due to the gain-switching operation principle. Gain switching must include a sudden change in carrier density and the carrier-induced refractive index changes in a resonator during pulse generation[23]. In the main part of the optical pulse, strong stimulated radiation leads to a decrease in carrier density and hence an increase in refractive index, resulting in a decrease of the oscillation frequency. The fast change of transient frequency in time domain significantly limits the pulse width. As shown in Fig. 4a, the pulse widths are only approximately 10 ps below 543.4 nm but they rapidly increase at wavelengths above 543.4 nm. Such complex spectral dynamics makes it very difficult to obtain short pulses from gain-switched semiconductor lasers. Thus, it is highly desirable to understand the dynamic characteristics of gain-switched pulses from perovskite lasers for ultrashort pulse generation. Figure 4b presents the log-log plots of the normalized output pulse waveforms at elevated pump fluences, showing typical gain-switching characteristics, i.e., clear exponential rise and decay of the output pulses. The delay times (squares), rise times (circles) and pulse widths/FWHMs (diamonds) of these gain-switched short pulses extracted from the experimental data are summarized in Fig. 4c, d. It can be seen that they gradually decreased

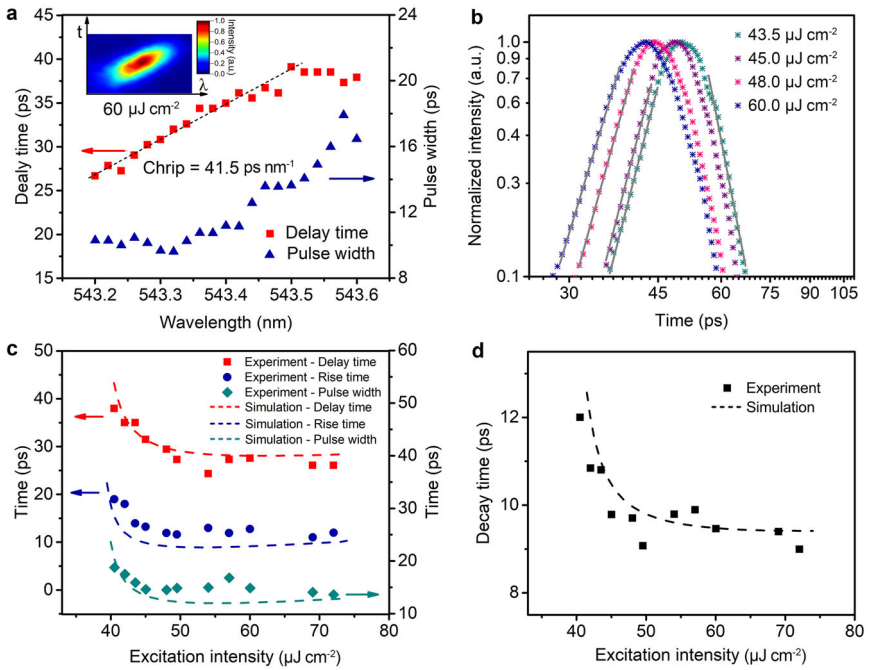


**Fig. 4 Gain-switching characteristics of output pulses in $CsPbBr_3$ microwires. a** Delay time and pulse width of optical pulse at 60 μJ $cm^{-2}$ with respect to wavelength. The error bars that represent the standard deviation from the mean are too small to be visible. The inset shows the streak camera image at 60 μJ $cm^{-2}$. **b** Normalized log-log plots of gain-switched pulse waveforms in Fig. 3. An exponential model (gray solid lines) fits well to the experimental data. The excitation energy-dependent delay time (red squares), rise time (circles), pulse width (diamonds) (**c**) and decay time (black squares) (**d**) of gain-switched pulses. The error bars here are too small to be visible. Dashed curves show the simulation results.

under progressively higher excitation fluences and eventually saturated to a lower minimum with further increasing the pump density. The shortest delay time and pulse width were limited to 26 and 13.6 ps, respectively. Such excitation fluence dependences of output laser pulses have been widely observed in other gain-switched semiconductor lasers[44–46], providing clear signatures of gain-switched lasing behaviors in $CsPbBr_3$ microwires.

**Rate equation analysis of gain-switched laser outputs**. The interaction between carrier and photon determines the properties of output pulse in stimulated emission process. For better understanding the gain-switched lasing behavior in the transient pumping regime and clarifying the factors in the pulse width limitations of the $CsPbBr_3$ microwires, a modified single-mode laser rate equation analysis[35] was carried out with taking gain nonlinearities and carrier recombination *ABC* model into account. The rate equation model can be described as following,

$$\frac{dn}{dt} = \frac{p(t)}{\hbar v \sigma} - \Gamma v_g g \frac{s}{1+\varepsilon s} - An - Bn^2 - Cn^3 \quad (1)$$

$$\frac{ds}{dt} = \Gamma v_g g \frac{s}{1+\varepsilon s} - \frac{s}{\tau_p} + \beta Bn^2 \quad (2)$$

$$g = g_0(n-n_0)\left[1 + \frac{g_0(n-n_0)}{g_s}\right]^{-1} \quad (3)$$

where $n$ is the carrier density, $p(t)$ is the transient optical pumping power given by a Gaussian distribution with a pulse duration of 0.5 ps, $\hbar v$ and $\sigma$ are respectively the pump photon energy and pump area in the $CsPbBr_3$ microwires, $\Gamma$ is the confinement factor, $v_g$ is the group velocity, $g$ is the carrier-density-dependent nonlinear material gain defined by a function of $g_s$ (saturated gain), $g_0$ (differential gain) and $n_0$ (transparent carrier density), $s$ is the photon density, $\varepsilon$ is the gain compression factor, $\beta$ is the spontaneous emission coupling factor, and $\tau_p$ denotes the photon lifetime.

Here, we use semi-quantitive numerical simulations to fit the experimental results because there still exist some unknown parameters in these rate equations. The pump area $\sigma$ is about $1.03 \times 10^{-5}$ $cm^2$ and the $v_g$ is $6.02 \times 10^{-3}$ cm ps$^{-1}$ [47]. The spontaneous emission coupling factor $\beta$ was 0.09 as estimated from Fig. 2e. We plausibly assumed $\Gamma = 1$, because the $CsPbBr_3$ microwires act as not only gain materials but also high-quality resonators. For the simulations, the saturated gain $g_s$, differential gain $g_0$, and gain compression factor $\varepsilon$ are three primary variations that were continuously modulated to match the simulation results with the experimental data shown in Fig. 4c, d. Generally, the saturated gain $g_s$ significantly affects the delay time and rise time but has almost no effect on decay time of the output laser pulses. When $g_s$ is fixed, the pulse shape hardly changes with varying the differential gain $g_0$, while the gain compression factor $\varepsilon$ suppresses the pulse peak but has almost no obvious effect on the rise time[34]. The numerical calculation process was performed iteratively until the simulation converges to self-consistent results.

As is known, the complicated intrinsic gain nonlinearities have a strong influence on the dynamical characteristics of semiconductor lasers, including dynamic frequency chirping, stability and pulse shaping of lasers[33], especially under high-density pulsed injection. And the carrier recombination plays an important role during gain-switching[35]. Consequently, the gain saturation and gain compression that reflect the gain nonlinearities, and the carrier recombination *ABC* model are ingeniously introduced into the rate equation model in our case to analyze the gain-switching characteristics of a perovskite microwire laser. In the simulations, the saturated gain $g_s$, differential gain $g_0$, and gain compression factor $\varepsilon$ are continuously adjusted within a

reasonable range under gain-switching operations. The best fitting results (dashed curves) can be obtained with $g_s = 88\ cm^{-1}$, $g_0 = 0.6 \times 10^{-9}\ cm$, and $\varepsilon = 0.92 \times 10^{-12}\ cm$, as exhibited in Fig. 4c, d.

The photon lifetime $\tau_p$ within the cavity was calculated to be about 0.7 ps using the relationship of $\tau_p = Q/\omega$, where $Q$ is the cavity quality factor and $\omega$ is angular frequency[48]. However, such theoretical value usually deviates from the experimental one. According to the previous report[45], the decay time of output pulse is almost determined by the photon lifetime $\tau_p$, which means that the more appropriate value of $\tau_p$ in the simulations should derived from the experimental decay curve with slight adjustment. Resultly, the emplyed $\tau_p$ in the simulations are chosen to be very close to the experimental decay time but not the theoretical one by $\tau_p = Q/\omega$. It was found that only when $g_s$ is around $88\ cm^{-1}$, the simulation results of rise time and delay time can be consistent with the experimental data, implying that $g_s$ plays a crucial role in determining the rise time and delay time, which is in good agreements with our previous study[45]. All parameters used in the calculation are summarized in Table 1.

It's worth noting that such a saturated gain of $g_s = 88\ cm^{-1}$ is far less than the gain values ($350–1200\ cm^{-1}$) from $CsPbBr_3$ perovskite by a variable stripe-length method[49,50]. When we assumed that $g_s$ is larger than 300, consistency between experimental and simulation results cannot be achieved for any choice of other parameters. The small value of saturated gain is considered to be caused by some nonlinear properties under gain-switching operations. In previous studies, some possible origins responsible for the nonlinearities have been discussed, and the most possible physical mechanisms focus on spectral hole burning and carrier heating[33]. In our condition, the carrier density rise sharply in an ultra-short time interval during gain-switching process under fs laser pumping, which may eventually result in an elevation of transient carrier temperature in the $CsPbBr_3$ microwire. The dynamical carrier temperature can be estimated by fitting the exponential high-energy tail of temporally and spectrally-resolved PL spectrum described by the relationship of emission intensity $I(\hbar\nu) \propto \exp(-\hbar\nu/kT)$[46,51], where $I(\hbar\nu)$ denotes emission intensity, $k$ is Boltzmann factor, and $T$ is the carrier temperature. The estimated carrier temperatures were 380 and 460 K under excitation energy of 0.4 $P_{th}$ and 0.9 $P_{th}$, respectively (see Supplementary Note 2, Supplementary Fig. 3). Therefore, the carrier heating should be the most possibly additional dynamical gain-suppression parameter that gives rise to the reduction of saturated gain in the present work. Since the low saturated gain can significantly increase the pulse width of gain-switched pulses, we can reasonably conclude that the carrier heating may be another possible reason for limiting the generation of shorter pulse in the $CsPbBr_3$ microwires laser.

**Table 1 Definitions and values of simulation parameters.**

| Parameters | Definitions | Values |
|---|---|---|
| $\sigma$ | Pump area | $1.03 \times 10^{-5}\ cm^2$ |
| $\hbar\nu$ | Pump photon energy | 2.28 eV |
| $\Gamma$ | Confinement factor | 1 |
| $v_g$ | Group velocity | $6.02 \times 10^{-3}\ cm\ ps^{-1}$ |
| $\tau_p$ | Photon lifetime | 8.5 ps |
| $\beta$ | Spontaneous emission coupling factor | 0.09 |
| $n_0$ | Transparent carrier density | $0.7 \times 10^{12}\ cm^{-2}$ |
| $g_s$ | Saturated gain | $88\ cm^{-1}$ |
| $g_0$ | Differential gain | $0.6 \times 10^{-9}\ cm$ |
| $\varepsilon$ | Gain compression factor | $0.92 \times 10^{-12}\ cm^2$ |
| $A$ | Shockley–Read–Hall coefficient | $7.0 \times 10^{-6}\ ps^{-1}$ |
| $B$ | Radiative coefficient | $9.8 \times 10^{-5}\ cm^2\ ps^{-1}$ |
| $C$ | Auger coefficient | $9.0 \times 10^{-6}\ cm^4\ ps^{-1}$ |

## Conclusions

In summary, a single-mode lasing behavior is observed from $CsPbBr_3$ microwires under fs optical pumping. The output laser pulses are investigated with streak camera measurements at various excitation intensities, and clear gain-switching mechanism for the short pulse generation are revealed. The shortest green pulse is obtained as short as 13.6 ps without any post-processing. To insight into the gain-switching dynamics of the $CsPbBr_3$ perovskite, we use a rate equation model combining with gain nonlinearities and carrier recombination $ABC$ model to semi-quantitatively simulate the excitation intensity dependencies of the delay time, pulse width, and rise time of the output laser pulses. A close consistency is obtained between the experimental and simulation results by continuously adjusting the three parameters of saturated gain $g_s$, differential gain $g_0$, and gain compression factor $\varepsilon$. Moreover, it is found that the carrier heating is a possible reason for the low saturated gain during gain-switching and hence limits the pulse width of the output pulses from the perovskite microwires. These results open the door of gain switching for perovskite lasers and provide a significant guidance for understanding generation dynamics and limit factors of short pulses.

## Methods

**Synthesis of $CsPbBr_3$ perovskite microwires**. The compounds $CsPbBr_3$ perovskite microwires were synthesized using a liquid-phase recrystallization method in an ambient environment. The 40 mmol $L^{-1}$ *N,N'*-dimethylformamide (DMF)-$CsPbBr_3$ precursor solution was prepared by mixing $PbBr_2$ (0.4 mmol) and CsBr (0.4 mmol) powders in 10 mL DMF solution. Then, the mixed solution was magnetically stirred for 4 h at a temperature of 70 °C. Next, 30 μL DMF-$CsPbBr_3$ solution was dip-cast onto a sapphire ($Al_2O_3$) substrate, which was preheated to a high temperature of 60 °C by a heater and keep the temperature unchanged to evaporate the solvent until the DMF solvent completely evaporated. The all-inorganic $CsPbBr_3$ microwires were successfully synthesized.

**Material characterization**. The morphology of synthesized $CsPbBr_3$ perovskite microstructures and luminescence signals were characterized respectively using scanning electron microscopy (SEM, XL30FEG, Philips, the Netherlands) and a charge-coupled device (CCD) camera. The elemental composition of the microwires was determined by energy dispersive X-ray spectroscopy (EDS, AMETEK EDAX). The crystal phase of the microwires was investigated using an X-ray diffraction (XRD) spectrometer (German Brook AXS D8 Discove). The UV–visible absorption spectra were measured using a Varian Cary 5000 spectrophotometer with an integrating sphere attachment in the range of 300–1000 nm.

**Optical measurements**. All the PL and TRPL experiments were performed with the home-built confocal $\mu$-PL system at room temperature (20 °C) by impulsive fs optical pumping at 400 nm. The 400-nm pulses were generated by frequency doubling the 800-nm fs pulses from a mode-locked Ti:sapphire regenerative amplifier (Verdi G8, Coherent, America) with 35-fs pulse duration and 1 kHz repetition rate. The pump beam was focalized to a diameter of 36 μm. The PL signals were detected by a triple-grating spectrometer (SR303, Andor) with an electrically-cooled CCD. The limited resolution of the spectrometer is 0.05 nm for the PL measurements. The TRPL was detected via a streak camera system (Hamamatsu, C10910) with a temporal resolution of ~5 ps. The 800 nm pulses with 80 MHz repetition rate, which emitted from the mode-locked Ti:sapphire laser, is converted into electrical signal as trigger signal of delay unit (C12270-01) by a PIN diode (C1808-03). The excitation-fluence-dependent PL signals in the TRPL measurements were detected by a spectrometer (HRS-300) and then collected by a streak camera with a digital CMOS camera through scanning of electric and magnetic fields.

**Reporting summary**. Further information on research design is available in the Nature Research Reporting Summary linked to this article.

## Data availability

All data in this study are available from the corresponding authors upon reasonable request.

Received: 18 November 2021; Accepted: 7 June 2022;
Published online: 23 June 2022

## References


1. Green, M. A., Ho-Baillie, A. & Snaith, H. J. The emergence of perovskite solar cells. *Nat. Photonics* **8**, 506–514 (2014).
2. Stranks, S. D. & Snaith, H. J. Metal-halide perovskites for photovoltaic and light-emitting devices. *Nat. Nanotechnol.* **10**, 391–402 (2015).
3. Lin, K. B. et al. Perovskite light-emitting diodes with external quantum efficiency exceeding 20 per cent. *Nature* **562**, 245–248 (2018).
4. Kovalenko, M. V., Protesescu, L. & Bodnarchuk, M. I. Properties and potential optoelectronic applications of lead halide perovskite nanocrystals. *Science* **358**, 745–750 (2017).
5. Yakunin, S. et al. Low-threshold amplified spontaneous emission and lasing from colloidal nanocrystals of cesium lead halide perovskites. *Nat. Commun.* **6**, 8056 (2015).
6. Fu, Y. P. et al. Broad wavelength tunable robust lasing from single-crystal nanowires of cesium lead halide perovskites ($CsPbX_3$, X=Cl, Br, I). *ACS Nano* **10**, 7963–7972 (2016).
7. Zheng, Z. et al. Space-confined synthesis of 2D all-inorganic $CsPbI_3$ perovskite nanosheets for multiphoton-pumped lasing. *Adv. Optical Mater.* **6**, 1800879 (2018).
8. Tang, B. et al. Single-mode lasers based on cesium lead halide perovskite submicron spheres. *ACS Nano* **11**, 10681–10688 (2017).
9. Li, X. J. et al. Solution-processed perovskite microdisk for coherent light emission. *Adv. Optical Mater.* **7**, 1900678 (2019).
10. Huang, C. Y. et al. $CsPbBr_3$ perovskite quantum dot vertical cavity lasers with low threshold and high stability. *ACS Photonics* **4**, 2281–2289 (2017).
11. Fu, A. & Yang, P. D. Organic−inorganic perovskites: Lower threshold for nanowire lasers. *Nat. Mater.* **14**, 557–558 (2015).
12. Eaton, S. W. et al. Lasing in robust cesium lead halide perovskite nanowires. *Proc. Natl Acad. Sci. USA* **113**, 1993–1998 (2016).
13. Liu, P. et al. Organic−inorganic hybrid perovskite nanowire laser arrays. *ACS Nano* **11**, 5766–5773 (2017).
14. Wang, X. X. et al. High-quality in-plane aligned $CsPbX_3$ perovskite nanowire lasers with composition-dependent strong exciton-photon coupling. *ACS Nano* **12**, 6170–6178 (2018).
15. Zhang, Q. et al. High-quality whispering-gallery-mode lasing from cesium lead halide perovskite nanoplatelets. *Adv. Funct. Mater.* **26**, 6238–6245 (2016).
16. Liao, Q., Hu, K., Zhang, H. H., Wang, X. D., Yao, J. N. & Fu, H. B. Perovskite microdisk microlasers self-assembled from solution. *Adv. Mater.* **27**, 3405–3410 (2015).
17. He, X. X. et al. Patterning multicolored microdisk laser arrays of cesium lead halide perovskite. *Adv. Mater.* **29**, 1604510 (2017).
18. Zhizhchenko, A. et al. Single-mode lasing from imprinted halide perovskite microdisks. *ACS Nano* **13**, 4140–4147 (2019).
19. Mamoori, F. A. IQ 532 Micropulse green laser treatment for refractory chronic central serous retinopathy. *Eye Care Vis.* **1**, 1–3 (2017).
20. Liu, X. Y. et al. 34.5 m underwater optical wireless communication with 2.70 Gbps data rate based on a green laser diode with NRZ-OOK modulation. *Opt. Express* **25**, 27937–27947 (2017).
21. Yu, T., Shu, S. J. & Chen, W. B. High repetition rate Tm:Ho:LuLiF master-oscillator and Tm-doped fiber power-amplifier system. *Chin. Opt. Lett.* **9**, 041407 (2011).
22. Krylov, A. A., Chernysheva, M. A., Chernykh, D. S. & Tupitsyn, I. M. A high power MOPA-laser based on a mode-locked thulium-doped fiber oscillator with intracavity dispersion management. *Laser Phys.* **23**, 045108 (2013).
23. Wada, K., Takamatsu, S., Watanabe, H., Matsuyama, T. & Horinaka, H. Pulse-shaping of gain-switched pulse from multimode laser diode using fiber Sagnac interferometer. *Opt. Express* **16**, 19872–19881 (2008).
24. Chen, S. Q. et al. Dynamics of short-pulse generation via spectral filtering from intensely excited gain-switched 1.55-mm distributed-feedback laser diodes. *Opt. Express* **21**, 10597–10605 (2013).
25. Takada, A., Sugie, T. & Saruwatari, M. High-speed picosecond optical pulse compression from gain-switched 1.3-mm distributed feedback-laser diode (DFBLD) through highly dispersive single-mode fiber. *J. Lightwave Technol.* **5**, 1525–1533 (1987).
26. Ahmed, K. A., Eggleton, B. J., Liu, H. F., Krug, P. A. & Ouellette, F. Simultaneous mode selection and pulse compression of gain-switched pulses from a Fabry-Perot laser using a 40-mm chirped optical fiber grating. *IEEE Photon. Technol. Lett.* **7**, 158–160 (1995).
27. Asahara, A. et al. Direct generation of 2-ps blue pulses from gain-switched InGaN VCSEL assessed by up-conversion technique. *Sci. Rep.* **4**, 6401 (2014).
28. Takada, A., Sugie, T. & Saruwatari, M. Transform-limited 5.6 ps optical pulse generation at 12 GHz repetition rate from gain-switched distributed feedback laser diode by employing pulse compression technique. *Electron. Lett.* **22**, 1347–1348 (1986).
29. Chen, S. Q. et al. Sub-5-ps optical pulse generation from a 1.55-μm distributed-feedback laser diode with nanosecond electric pulse excitation and spectral filtering. *Opt. Express* **20**, 2483–2489 (2012).
30. Chen, S. Q. et al. Blue 6-ps short-pulse generation in gain-switched InGaN vertical-cavity surface-emitting lasers via impulsive optical pumping. *Appl. Phys. Lett.* **101**, 191108 (2012).
31. Huikari, J. M. T., Avrutin, E. A., Ryvkin, B. S., Nissinen, J. J. & Kostamovaara, J. T. High-energy picosecond pulse generation by gain switching in asymmetric waveguide structure multiple quantum well lasers. *IEEE J. Sel. Top. Quantum Electron* **21**, 189–194 (2015).
32. Ito, T. et al. Femtosecond pulse generation beyond photon lifetime limit in gain-switched semiconductor lasers. *Commun. Phys.* **1**, 42 (2018).
33. Huang, J. & Casperson, L. W. Gain and saturation in semiconductor lasers. *Opt. Quantum Electron.* **25**, 369–390 (1993).
34. Chen, S. Q. et al. Analysis of gain-switching characteristics including strong gain saturation effects in low-dimensional semiconductor lasers. *Jpn. J. Appl. Phys.* **51**, 098001 (2012).
35. Bao, X. M., Liu, Y. J., Weng, G. E., Hu, X. B. & Chen, S. Q. ABC-model analysis of gain-switched pulse characteristics in low-dimensional semiconductor lasers. *Quantum Electron* **48**, 7–12 (2018).
36. Glezer, E. N. et al. Three-dimensional optical storage inside transparent materials. *Opt. Lett.* **21**, 2023–2025 (1996).
37. Melcer, L. G., Karin, J. R., Nagarajan, R. & Bowers, J. E. Picosecond dynamics of optical gain vertical cavity surface emitting switching in lasers. *IEEE J. Quantum Electron* **27**, 1417–1425 (1991).
38. Wang, X. X. et al. Cesium lead halide perovskite triangular nanorods as high-gain medium and effective cavities for multiphoton-pumped lasing. *Nano Res.* **10**, 3385–3395 (2017).
39. Hua, B., Motohisa, J., Kobayashi, Y., Hara, S. & Fukui, T. Single GaAs/GaAsP coaxial core-shell nanowire lasers. *Nano Lett.* **9**, 112–116 (2009).
40. Johnson, J. C., Yan, H. Q., Yang, P. D. & Saykally, R. J. Optical cavity effects in ZnO nanowire lasers and waveguides. *J. Phys. Chem. B* **107**, 8816–8828 (2003).
41. Yang, Z. et al. Controllable growth of aligned monocrystalline $CsPbBr_3$ microwire arrays for piezoelectric-induced dynamic modulation of single-mode lasing. *Adv. Mater.* **31**, 1900647 (2019).
42. Wei, Q. et al. Recent progress in metal halide perovskite micro-and nanolasers. *Adv. Optical Mater.* **7**, 1900080 (2019).
43. Chen, S. T., Zhang, C., Lee, J., Han, J. & Nurmikko, A. High-Q, low-threshold monolithic perovskite thin-film vertical-cavity lasers. *Adv. Mater.* **29**, 1604781 (2017).
44. Paulus, P., Langenhorst, R. & Jäger, D. Generation and optimum control of picosecond optical pulses from gain-switched semiconductor lasers. *IEEE J. Quantum Electron* **24**, 1519–1523 (1988).
45. Chen, S. Q. et al. Spectral dynamics of picosecond gain-switched pulses from nitride-based vertical-cavity surface-emitting lasers. *Sci. Rep.* **4**, 4325 (2014).
46. Ito, T. et al. Transient hot-carrier optical gain in a gain-switched semiconductor laser. *Appl. Phys. Lett.* **103**, 082117 (2013).
47. Shang, Q. Y. et al. Enhanced optical absorption and slowed light of reduced-dimensional $CsPbBr_3$ nanowire crystal by exciton−polariton. *Nano Lett.* **20**, 1023–1032 (2020).
48. Yariv, A. & Yeh, P. *Photonics: optical electronics in modern communications* 6th edn. (Oxford University Press, Oxford, 2007).
49. Qaid, S. M. H., Ghaithan, H. M., Al-Asbahi, B. A. & Aldwayyan, A. S. Achieving optical gain of the $CsPbBr_3$ perovskite quantum dots and influence of the variable stripe length method. *ACS Omega* **6**, 5297–5309 (2021).
50. Zhong, Y. G. et al. Large-scale thin $CsPbBr_3$ single-crystal film grown on sapphire via chemical vapor deposition: toward laser array application. *ACS Nano* **14**, 15605–15615 (2020).
51. Leo, K., Rühle, W. W., Queisser, H. J. & Ploog, K. Reduced dimensionality of hot-carrier relaxation in GaAs quantum wells. *Phys. Rev. B* **37**, 7121–7124 (1988).


## Acknowledgements

The authors acknowledge the financial support from the National Natural Science Foundation of China (Grant no. 61874044), the National Key Research and Development Project of China (Grant no. 2019YFB1503402), and the 111 project of China (Grant no. B12024). This work was also partly supported by KAKENHI Grant no. 21H01361 from the Japan Society for the Promotion of Science (JSPS).

## Author contributions

S.Q.C. conceived the idea of studying gain switching in $CsPbBr_3$ perovskite microwires. S.Q.C., G.W., and J.T. proposed the strategy and designed the experiments. J.T., S.J.C., and G.W. synthesized the investigated $CsPbBr_3$ microwires. J.T., G.W., and Y.L. performed structural characterizations of the samples. G.W. and J.T. constructed the optical

experimental setup. J.T., G.W., Y.L., and S.J.C. carried out the optical measurements with help from X.H., X.L., and C.Z. Y.L., J.T., and F.C. performed the rate equation simulation. J.T. and G.W. wrote the manuscript with suggestions from S.Q.C., J.C., and H.A. All authors extensively discussed the results.

## Competing interests

The authors declare no competing interests.

## Additional information

**Supplementary information** The online version contains supplementary material available at https://doi.org/10.1038/s42005-022-00938-8.

**Correspondence** and requests for materials should be addressed to Guoen Weng or Shaoqiang Chen.

**Peer review information** *Communications Physics* thanks Wan Maryam and the other, anonymous, reviewer(s) for their contribution to the peer review of this work. Peer reviewer reports are available.

**Reprints and permission information** is available at http://www.nature.com/reprints

**Publisher's note** Springer Nature remains neutral with regard to jurisdictional claims in published maps and institutional affiliations.